J|A|C|S

A R T I C L E S

New Model for a Theoretical Density Functional Theory Investigation of the Mechanism of the Carbonic Anhydrase: How Does the Internal Bicarbonate Rearrangement Occur?

Andrea Bottoni,*,[†] Camilla Zaira Lanza,[‡] Gian Pietro Miscione,[†] and Domenico Spinelli[‡]

Contribution from the Dipartimento di Chimica "G. Ciamician", Universitá di Bologna, via Selmi 2, 40126 Bologna, Italy, and the Dipartimento di Chimica Organica "A. Mangini", Universitá di Bologna, via S. Donato 15, 40127 Bologna, Italy

Received June 2, 2003; Revised Manuscript Received October 27, 2003; E-mail: andrea@ciamserv.ciam.unibo.it

Abstract: A theoretical density functional theory (DFT, B3LYP) investigation has been carried out on the catalytic cycle of the carbonic anhydrase. A model system including the Glu106 and Thr199 residues and the "deep" water molecule has been used. It has been found that the nucleophilic attack of the zinc-bound OH on the CO_2 molecule has a negligible barrier (only 1.2 kcal mol^{-1}). This small value is due to a hydrogen-bond network involving Glu106, Thr199, and the deep water molecule. The two usually proposed mechanisms for the internal bicarbonate rearrangement have been carefully examined. In the presence of the two Glu106 and Thr199 residues, the direct proton transfer (Lipscomb mechanism) is a two-step process, which proceeds via a proton relay network characterized by two activation barriers of 4.4 and 9.0 kcal mol^{-1}. This pathway can effectively compete with a rotational mechanism (Lindskog mechanism), which has a barrier of 13.2 kcal mol^{-1}. The fast proton transfer found here is basically due to the effect of the Glu106 residue, which stabilizes an intermediate situation where the Glu106 fragment is protonated. In the absence of Glu106, the barrier for the proton transfer is much larger (32.3 kcal mol^{-1}) and the Lindskog mechanism becomes favored.

Introduction

Carbonic anhydrases (CA) are a class of zinc-based metalloenzymes that catalyze the reversible hydration of CO_2 to bicarbonate and a proton. Human carbonic anhydrase II (HCAII), which is present in nonpigmented epithelial cells of the eye and red blood cells, is a single polypeptide chain of 260 amino acids. It is the most efficient of the seven known isozymes found in vertebrates and catalyzes the reaction with rates up to 10^7 times higher than in the uncatalyzed case.[1-3] X-ray diffraction techniques[4-7] have shown that the active site consists of a zinc cation (Zn^{2+}) firmly bound to three rigid imidazole groups belonging to three histidine residues (His94, His96, and His119). A water molecule completes the nearly symmetrical tetrahedral coordination geometry of the metal. The active site is near the apex of a conical cavity, which is 15 Å deep and 15 Å wide at the base and divides into a hydrophilic
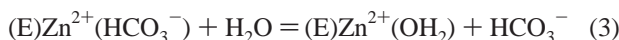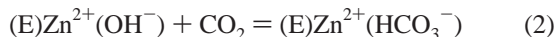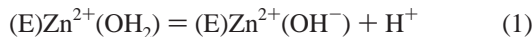
and hydrophobic pocket. The hydrophilic region contains the group His64 and several water molecules. The His64 residue is thought to be involved as a proton acceptor in the migration of the proton from the zinc-bound water to the external buffer. The hydrophobic pocket provides binding sites for the CO_2 transport and contains the so-called "deep water". This molecule, which is about 3.2 Å away from the zinc ion, is thought to be displaced by CO_2 during the substrate binding.

Over the last three decades, the catalytic mechanism of carbonic anhydrase has been the subject of a large number of experimental[1-14] and theoretical[15-30] investigations. The almost

† Dipartimento di Chimica "G. Ciamician", Universitá di Bologna.
‡ Dipartimento di Chimica Organica "A. Mangini", Universitá di Bologna.

(1) Bertini, I.; Luchinat, C. *Acc. Chem. Res.* **1983**, *16*, 272.
(2) Silverman, D. N.; Lindskog, S. *Acc. Chem. Res.* **1988**, *21*, 30.
(3) Christianson, D. W.; Fierke, C. A. *Acc. Chem. Res.* **1996**, *29*, 331 and references therein.
(4) Woolley, P. *Nature* **1975**, *258*, 677.
(5) Liljas, A.; Kannan, K. K.; Bergsten, P. C.; Waara, I.; Friborg, K.; Strandberg, B.; Carlbom, U.; Jarup, L.; Lovgren, S.; Petef, M. *Nat. New Biol.* **1972**, *235*, 131.
(6) Eriksson, E. A., Jones, T. A.; Liljas, A. In *Zinc Enzymes*; Bertini, I., Luchinat, C., Maret, W., Zappezauer, M., Eds.; Birkhauser: Boston, MA, 1986; Vol. 1, p 317.
(7) Hakansson, K.; Carlsson, M.; Svensson, L. A.; Liljas, A. *J. Mol. Biol.* **1992**, *227*, 1192.

(8) Kimura, E. *Acc. Chem. Res.* **2001**, *34*, 171 and references therein.
(9) Huang, C.; Lesburg, C. A.; Kiefer, L. L.; Fierke, C. A.; Christianson, D. W. *Biochemistry* **1996**, *35*, 3439.
(10) Lesburg, C. A.; Huang, C.; Christianson, D. W.; Fierke, C. A. *Biochemistry* **1997**, *36*, 15780.
(11) Zhang, X.; Hubbard, C. D.; van Eldik, R. *J. Phys. Chem.* **1996**, *100*, 9161.
(12) Nair, S. K.; Calderone, T. L.; Christianson, D. W.; Fierke, C. A. *J. Biol. Chem.* **1991**, *266*, 17320.
(13) Tu, C.; Tripp, B. C.; Ferry, J. G.; Silverman, D. N. *J. Am. Chem. Soc.* **2001**, *123*, 5861.
(14) Thomas, S. *J. Theor. Biol.* **2002**, *215*, 399.
(15) (a) Liang, J.-Y.; Lipscomb, W. N. *J. Am. Chem. Soc.* **1986**, *108*, 5053. (b) Liang, J.-Y.; Lipscomb, W. N. *Biochemistry* **1987**, *26*, 5293.
(16) Merz, K. M.; Hoffmann, R.; Dewar, M. J. S. *J. Am. Chem. Soc.* **1989**, *111*, 5636.
(17) Liang, J.-Y.; Lipscomb, W. N. *Int. J. Quantum Chem.* **1989**, *36*, 299.
(18) Jacob, O.; Cardenas, R.; Tapia, O. *J. Am. Chem. Soc.* **1990**, *112*, 8692.
(19) Krauss, M.; Garmer, D. R. *J. Am. Chem. Soc.* **1991**, *113*, 6426.
(20) Zheng, Y.-J.; Merz, K. M. *J. Am. Chem. Soc.* **1992**, *114*, 10498.
(21) Sola, M.; Lledos, A.; Duran, M.; Bertran, J. *J. Am. Chem. Soc.* **1992**, *114*, 869.
(22) Sakurai, M.; Furuki, T.; Inoue, Y. *J. Phys. Chem.* **1995**, *99*, 17789.
(23) Murcko, M. A. *Theor. Chem. Acc.* **1997**, *96*, 56.

universally accepted mechanism, which stems from these studies, consists of three main steps. The first step involves the proton release from the Zn-bound water to form Zn-bound hydroxide (see eq 1, where E stands for the enzyme). The second step is a nucleophilic attack by the Zn−OH unit on the carbon atom of CO_2 to form a bicarbonate (eq 2). In step 3, the zinc-bound bicarbonate is replaced by an external water molecule (eq 3), which is deprotonated to close the catalytic cycle.
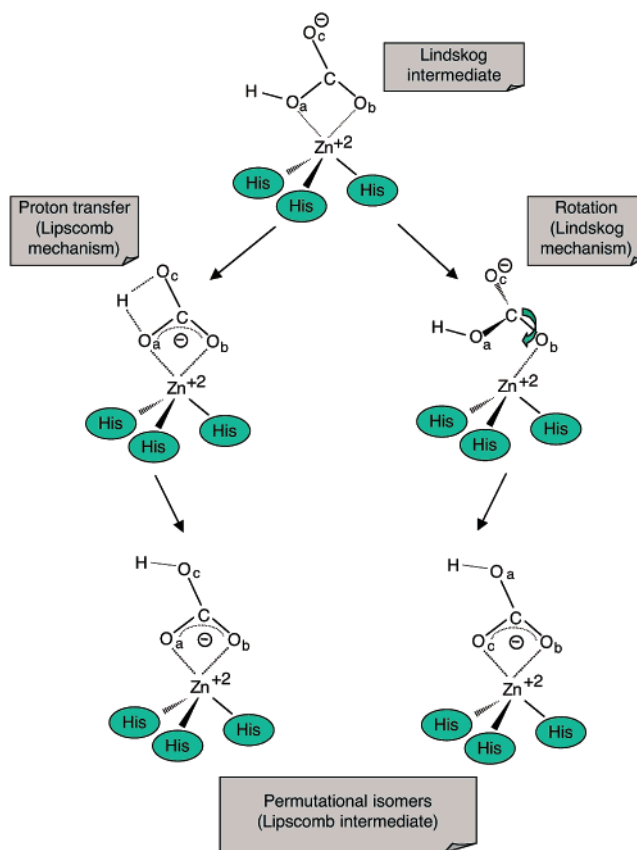
$$(E)Zn^{2+}(OH_2) = (E)Zn^{2+}(OH^-) + H^+ \qquad (1)$$

$$(E)Zn^{2+}(OH^-) + CO_2 = (E)Zn^{2+}(HCO_3^-) \qquad (2)$$

$$(E)Zn^{2+}(HCO_3^-) + H_2O = (E)Zn^{2+}(OH_2) + HCO_3^- \qquad (3)$$

An alternative mechanism has been very recently proposed by Thomas.[14] The model suggested by this author is based on the X-ray structure of the hydrogen-bond network in the catalytic site. Within this mechanistic scheme the nucleophilic attack on CO_2 is provided by the zinc-bound water molecule and not by the zinc-bound hydroxide. A simultaneous electrophilic activation of carbon dioxide is due to the formation of a low-barrier hydrogen-bond (LBHB) network that is supposed to lower the energy of the transition state for the C−O bond formation.

Studies based on solvent isotope effects have indicated as the rate-determining step of the mechanism shown in eqs 1−3 the proton transfer from the zinc-bound water to a proton acceptor in the active site (step 1, generation of the activated enzyme). The acceptor is thought to be the imidazole ring of the histidine residue His64.[2,16,30] Once the proton transfer is complete, the proton is then transferred to a buffer in the surrounding medium. It has also been conjectured that a proton relay involving Thr199 and Glu106 can work as a proton acceptor. Following this hypothesis, the zinc-bound water would give up a proton to threonine, which then would deliver a proton to Glu106.[16] However AM1 computations carried out by Merz et al.[16] were not able to locate a reaction path corresponding to this proton relay network. An alternative way to complete the catalytic cycle was suggested by the same authors on the basis of AM1 computations. They proposed that carbonic acid, rather than bicarbonate, is the final product of the hydration reaction and represents the leaving group of step 3. This molecule would play a role as a proton bridge between the active site and the His64 residue. Finally, in a very recent paper Cui and Karplus[30] carried out an accurate study on the energetics of the proton transfer from the zinc-bound water to the His64 residue, mediated by different numbers of water molecules. They found that a model involving three or four water molecules provide results that are consistent with the experimental kinetic observations.

In the most recent publications on the mechanism of action of CA, the attention has been focused on the details of the generally accepted reaction scheme corresponding to eqs 1−3.

(24) Merz, K. M.; Banci, L. *J. Am. Chem. Soc.* **1997**, *119*, 863.
(25) Lu, D.; Voth, G. A. *J. Am. Chem. Soc.* **1998**, *120*, 4006.
(26) Toba, S.; Colombo, G.; Merz, K. M. *J. Am. Chem. Soc.* **1999**, *121*, 2290.
(27) Denisov, V. P.; Jonsson, B.-H.; Halle, B. *J. Am. Chem. Soc.* **1999**, *121*, 2327.
(28) Mauksch, M.; Brauer, M.; Weston, J.; Anders, E. *ChemBioChem* **2001**, *2*, 190.
(29) Brauer, M.; Perez-Lustres, J. L.; Weston, J.; Anders, E. *Inorg. Chem.* **2002**, *41*, 1454.
(30) Cui, Q.; Karplus, M. *J. Phys. Chem. B* **2003**, *107*, 1071.

Scheme 1

In particular, the structural rearrangement and the consequent stabilization of the bicarbonate product obtained in step 2 (Lindskog intermediate) have been extensively investigated. It has been suggested that this rearrangement can occur via two alternative paths, known as the Lipscomb and Lindskog mechanisms (see Scheme 1). The former corresponds to a direct intramolecular proton transfer from the zinc-bound oxygen to another oxygen of the bicarbonate moiety. The latter does not involve any proton transfer but rather a change of the oxygen atom directly coordinated to the zinc ion. Zheng and Merz[20] suggested that in this case the rearrangement can occur via an inner rotation of the bicarbonate around a carbon−oxygen bond and for this process they computed a barrier of 4.1 kcal mol^{-1} at the MP2 level. The two mechanisms would lead to more stable identical permutation isomers (Lipscomb intermediate).[17]

The barrier for the direct internal proton transfer for a simple bicarbonate ion has been computed by Liang and Lipscomb[15] using PRDDO, HF/4-31G+, and MP2/4-31G approaches. They found a large barrier of 35.6 kcal mol^{-1} (PRDDO), which is reduced to 3.5 and 1.4 kcal mol^{-1} when one water and two water molecules, respectively, are included for the proton relay. They suggested that in the enzyme the Thr199 residue or solvent molecules could perform the relay function.

Bertran and co-workers[21] have compared the two possible rearrangement mechanisms at the HF and MP2 levels using a simple model system formed by $[(NH_3)_3Zn(OH)]^+$ and a CO_2 molecule. An additional water molecule, which can facilitate the proton relay (mainly in the Lipscomb mechanism), has been added to this system. These authors found that both mechanisms have activation energies that are compatible with the experimental data. They can compete in the enzymatic process, even

if the Lindskog pathway is slightly favored. The authors pointed out the need of using more precise models of the active site to study the reaction.

In a recent paper Anders and co-workers[28] have examined the complete reaction path for this enzymatic reaction at the B3LYP/6-311+G** level. To mimic the active center of the enzyme, they have used the model system $[(NH_3)_3Zn(OH)]^+$, which reacts with a CO_2 molecule. They concluded that the rate-determining step of the process is probably the nucleophilic attack of the Zn-bound OH on carbon dioxide and not, as commonly suggested, the proton transfer from the zinc-bound water. Also, they found that the rearrangement of the bicarbonate most likely occurs through a Lindskog-type mechanism (internal rotation) and does not involve a direct proton shift, which has a significantly higher activation energy (about 28 kcal mol^{-1}). In a subsequent paper[29] the same authors have examined at the DFT and PM3 levels a series of zinc complexes designed to mimic the carbonic anhydrase active site. The computational results indicate a mechanism that is general for all complexes. Activation barriers in the range 4−6 kcal mol^{-1} have been found for the nucleophilic attack. In all cases the equilibrium between the Lindskog and Lipscomb intermediates favors the latter one.

In the present paper we examine again some aspects of the mechanism of CA corresponding to eqs 1−3 and we leave for future investigations the alternative mechanism suggested by Thomas.[14] We believe that, despite the numerous studies available in the literature, many questions are still open. In our opinion the uncertainty concerning many mechanistic details, is determined by various factors. An important aspect is certainly the inadequacy of the up to now used quantum-mechanical model systems, where the closest residues to the HO−Zn fragment have been systematically missed. These residues, in particular Glu106 and Thr199, can play a key role in the mechanism of the bicarbonate rearrangement. Other residues can be vital in determining the direction of the nucleophilic attack (and the corresponding barrier) and the way the product moves away from the metal and abandons the active site. Another factor that is responsible of the weakness of many theoretical investigations is the full geometry optimization applied to the molecular systems that emulate the enzyme active site. This approach, which is correct in the study of organic reactions, introduces in a biosystem simulation degrees of freedom that are not truly present in the real enzyme and provides a misleading picture of many interactions. Finally, the unreliability of many investigations can be partly ascribed to the use of quantum-mechanical approaches where the correlation contributions are missed or where these contributions have been evaluated by noncorrelated structures (for instance, single-point MP2 computations on Hartree−Fock structures).[15,16,20,21]

Here we focus our attention on the following mechanistic aspects: (1) the nucleophilic attack of the zinc-bound hydroxide on CO_2, (2) the internal rearrangement of the resulting bicarbonate ion, and (3) the attack of a water molecule on the zinc−bicarbonate complex. To this purpose we use a model system that includes the Glu106 and Thr199 residues and the deep water molecule revealed in crystallographic studies. A detailed analysis of the effect of Glu106 and Thr199 is given.

2. Computational Details and Choice of the Model

The model system used here to emulate the HCAII active site (see Figure 1) has been assembled by use of the crystallographic structure
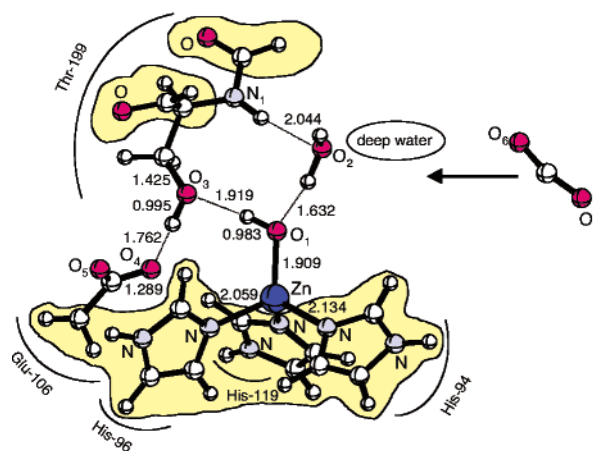
Figure 1. Schematic representation of the model system used in this paper (bond lengths in angstroms, angles in degrees). The contour lines mark the groups that are kept frozen during the geometry optimization. These groups are described by the STO-3G basis set. For the remaining atomic groups the DZVP basis has been used.

available in the literature (the Protein Data Bank code is 2CBA and the resolution is 1.54 Å).[7] This system includes (i) a Zn^{2+} cation bonded to a HO^- group and three imidazole rings belonging to the three histidine residues His94, His96, and His119; (ii) the Glu106 residue; (iii) the Thr199 residue; (iv) a water molecule (deep water); and (v) a CO_2 molecule. To reduce the size of the model, an acetate fragment has been used to emulate the Glu106 residue. Also, we have replaced the threonine with a serine and we have cut the protein backbone along the bonds adjacent to the two carbonyl groups.

To preserve the geometry of the active-site cavity and thus emulate the partially constraining effect of the protein environment, during the geometry optimization procedure we have fixed the positions of the atoms not directly involved in the reaction. These atoms have been anchored to their crystallographic coordinates and are marked by contour lines in Figure 1. For the serine/threonine residue we have not locked the whole CH_2−OH fragment. This should allow the OH group approximately the same freedom it has in the enzyme to adjust its position and form effective hydrogen bonds with the neighboring groups.

All the reported density functional theory (DFT) computations have been carried out with the Gaussian 98 series of programs[31] using the B3LYP[32] functional and locally dense basis sets (LDBS).[33] The B3LYP functional has been demonstrated to provide reliable description of systems including transition metals and involving hydrogen-bond interactions.[34,35] According to this approach, the system has been partitioned into two different regions, which were assigned basis sets of different accuracy. One region contains the atoms directly involved

(31) Frisch, M. J.; Trucks, G. W.; Schlegel, H. B.; Scuseria, E. G.; Robb, M. A.; Cheeseman, J. R.; Zakrzewski, V. G.; Montgomery, J. A.; Stratmann, R. E.; Burant, J. C.; Dapprich, S.; Millam, J. M.; Daniels, A. D.; Kudin, K. N.; Strain, M. C.; Farkas, O.; Tomasi, J.; Barone, V.; Cossi, M.; Cammi, R.; Mennucci, B.; Pomelli, C.; Adamo, C.; Clifford, S.; Ochterski, J.; Petersson, G. A.; Cui, Q.; Morokuma, K.; Malik, D. K.; Rabuck, A. D.; Raghavachari, K.; Foresman, J. B.; Cioslowski, J.; Ortiz, J. V.; Stefanov, B. B.; Liu, G.; Liashenko, A.; Piskorz, P.; Kamaromi, I.; Gomperts, R.; Martin, R. L.; Fox, D. J.; Keith, T.; Al-Laham, M. A.; Peng, C. Y.; Nanayakkara, A.; Gonzalez, C.; Challacombe, M.; Gill, P. M. W.; Johnson, B. G.; Chen, W.; Wong, M. W.; Andres, J. L.; Gonzalez, C.; Head-Gordon, M.; Replogle, E. S.; Pople, J. A. Gaussian 98, Revision A.6; Gaussian, Inc.: Pittsburgh, PA, 1998.
(32) Becke, A. D. *J. Chem. Phys.* **1993**, *98*, 5648.
(33) (a) DiLabio, G. A.; Pratt, D. A.; Wright, J. S. *Chem. Phys. Lett.* **1998**, *297*, 181. (b) Wright, J. S.; Johnson, E. R.; DiLabio, G. A. *J. Am. Chem. Soc.* **2001**, *123*, 1173.
(34) (a) Ziegler, T. *Chem. Rev.* **1991**, *91*, 651. (b) Fan, L.; Ziegler, T. *J. Am. Chem. Soc.* **1992**, *114*, 10890.
(35) (a) Bernardi, F.; Bottoni, A.; Miscione, G. P. *Organometallics* **2001**, *20*, 2751. (b) Bottoni, A.; Perez Higueruelo, A.; Miscione, G. P. *J. Am. Chem. Soc.* **2002**, *124*, 5506. (c) Bernardi, F.; Bottoni, A.; De Vivo, M.; Garavelli, M.; Keseru, G.; Naray-Szabo, G. *Chem. Phys. Lett.* **2002**, *362*, 1.
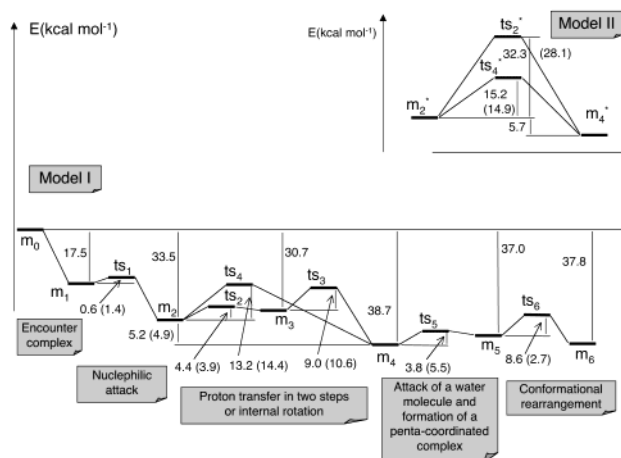
Figure 2. Energy profiles obtained for various steps of the catalytic process for the two model systems, I and II.

in the reaction or in the formation of hydrogen bonds (with the exception of the methylene group of the serine residue). The coordinates of these atoms are fully optimized. The other region includes all the remaining atoms, i.e., those atoms that are kept frozen during the geometry optimization. In the former case we have used the DZVP basis, which is a local spin density- (LSD-) optimized basis set of double-ζ quality.[36] This basis, which includes polarization functions, is suitable to describe weak hydrogen interactions such as those occurring in the system investigated here. In the latter case the small STO-3G basis set[31] has been employed. Furthermore, to obtain a more accurate estimate of the energetics of the reaction, we have carried out single-point computations on the previously optimized structures using the DZVP basis on the entire system. The transition vector of the various transition states has been analyzed by means of frequency computations.

The effect of the whole protein environment has been evaluated with the solvent continuous model approach COSMO[37] as implemented in the Turbomole package.[38] To this purpose the dielecric constant of nitromethane ($\epsilon = 38.2$) was used. This value has been chosen to take into account the simultaneous presence of hydrophilic and hydrophobic groups around the active site. A value of about 40 has been suggested elsewhere to take into account the effect of charge–charge interactions in proteins.[39] Several examples are available in the literature where the COSMO approach has been used in calculations on enzymatic models and systems involving hydrogen bonds and proton transfers.[40]

3. Results and Discussion

In this section we examine in detail the singlet potential surface obtained for the model system of Figure 1. We refer to this system as model I. The corresponding energy profile is reported in Figure 2, while the structures of the various critical points located along it are schematically represented in Figures 3–8. The results are discussed in sections A–C.

To elucidate the role played by the two residues Thr199 and Glu106, which have never been considered in previous works,
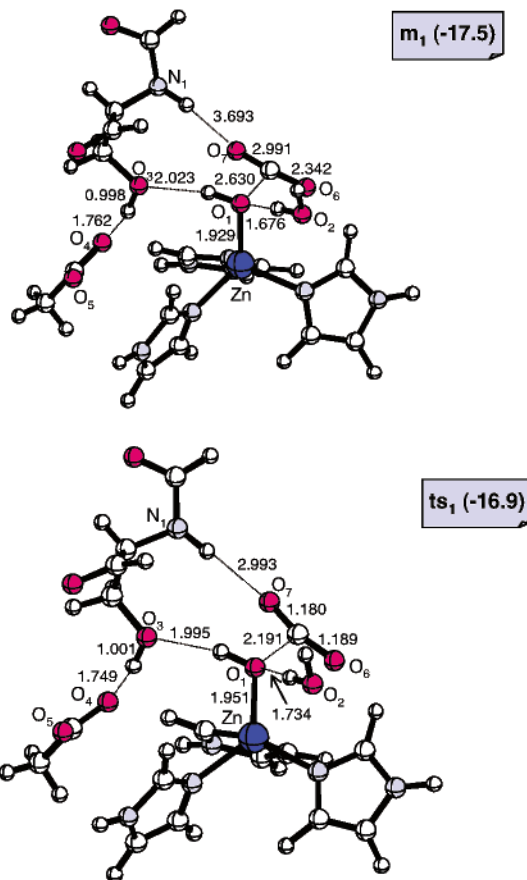
(36) (a) Godbout, N.; Salahub, D. R.; Andzelm, J.; Wimmer, E. *Can. J. Chem.* **1992**, *70*, 560. (b) UniChem DGauss, Version 2.3.1, 1994, Cray Research, Inc.
(37) (a) Klamnt, A. *J. Phys. Chem.* **1995**, *99*, 2224. (b) Klamnt, A. *J. Phys. Chem.* **1996**, *100*, 3349.
(38) Turbomole, version 5.6, Institut für Physikalische Chemie und Elektrochemie Lehrstuhl für Theoretische Chemie, Universität Karlsruhe, Kaiserstr. 12, D-76128 Karlsruhe.
(39) Warshel, A.; Naray-Szabo, G.; Sussman, F., Hwang, J.-K. *Biochemistry* **1989**, *28*, 3629.
(40) (a) Lau, E. Y.; Newby, Z. E.; Bruice, T. C. *J. Am. Chem. Soc.* **2001**, *123*, 3350. (b) Bach, R. D.; Thorpe, C.; Dmitrenko, O. *J. Phys. Chem B* **2002**, *106*, 4325. (c) Keeffe, J. R.; Gronert, S.; Colvin, M. E.; Tran, N. L. *J. Am. Chem. Soc.* **2003**, *125*, 11730. (d) Chocholousova, J.; Vacek, J.; Hobza, P. *J. Phys. Chem A* **2003**, *107*, 3086.
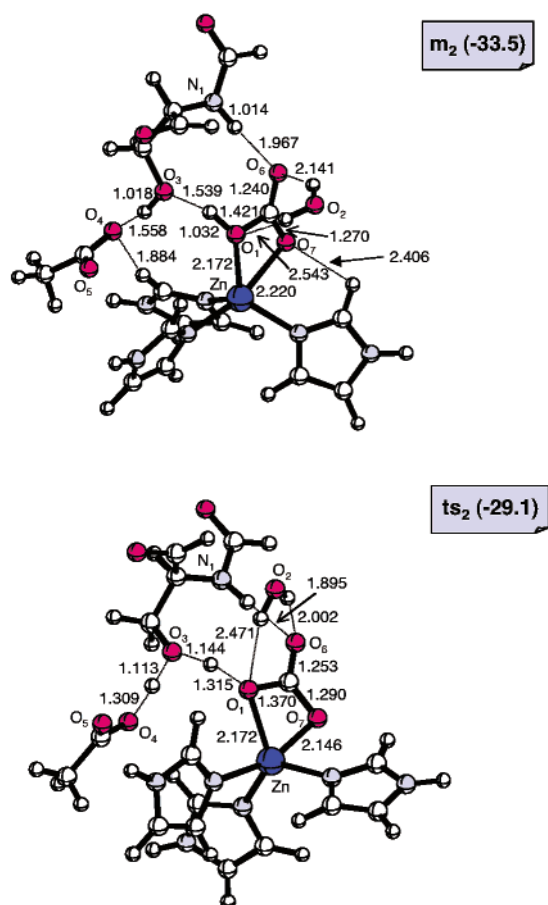

Figure 3. Schematic representation of the structures of the critical points $\mathbf{m_1}$ and $\mathbf{ts_1}$ (bond lengths in angstroms, angles in degrees). The energy values (kilocalories per mole) are relative to $\mathbf{m_0}$.

we have reinvestigated the bicarbonate internal rearrangement in the absence of Glu106. The model system where Glu106 is missed is referred as model II. The corresponding results are discussed in section D.

A. Nucleophilic Attack. In the first step of the catalytic reaction the CO_2 molecule forms with the CA active site a preliminary complex $\mathbf{m_1}$ (see Figure 3), where the OH lone pair interacts with the CO_2 carbon. To form $\mathbf{m_1}$, no activation barrier is required even if the CO_2 molecule pushes away the deep water and breaks the hydrogen bond between this molecule and the N_1–H fragment of the threonine moiety. The replacement of the deep water by CO_2 considerably stabilizes $\mathbf{m_1}$, this complex being 17.5 kcal mol^{-1} lower than the asymptotic limit $\mathbf{m_0}$. The other geometrical parameters do not change significantly on passing from $\mathbf{m_0}$ to $\mathbf{m_1}$: the hydrogen bond involving the glutamate and threonine residues remains almost identical, while that between the threonine and the zinc-bound OH group becomes slightly longer (2.023 Å). Thus, the stabilization is mainly due to the interaction between the OH lone pair and the electrophilic CO_2 carbon. A negligible barrier of 0.6 kcal mol^{-1} is required by the nucleophilic attack of the hydroxide on the CO_2 carbon. The corresponding transition state $\mathbf{ts_1}$ (Figure 3) is characterized by a newly formed O_1–C bond of 2.191 Å that causes a lengthening of the Zn–O_1 distance (from 1.929 Å in $\mathbf{m_1}$ to 1.951 Å in $\mathbf{ts_1}$). To explain the very small activation energy required by the nucleophilic attack, it is useful to compare the net charges on the zinc (0.65) and hydroxide oxygen (-1.01) in $\mathbf{m_1}$ to the corresponding values obtained for

Figure 4. Schematic representation of the structures of the critical points m_2 and ts_2 (bond lengths in angstroms, angles in degrees). The energy values (kilocalories per mole) are relative to m_0.

the simple system $[Zn(OH)]^+$ (1.15 and -0.63, respectively), where the imidazole ligands are missing. It is evident that the metal ligands considerably increase the oxygen negative charge and thus the nucleophilicity of the hydroxide group and cause a lowering of the barrier. The high oxygen charge density also provides an explanation for the strong interaction between the hydroxide lone pair and the CO_2 carbon and the consequent energy stabilization observed in m_1. Furthermore, it is worthwhile to consider the corresponding net charges obtained for the $[Zn(OH)(NH_3)_3]^+$ system, widely used in the literature to emulate the enzyme active site. These are 0.93 and -0.85 for zinc and oxygen, respectively, and clearly indicate that in the simple model system where the ammonia molecules emulate the imidazole rings, the hydroxide nucleophilicity is still significantly lower than that found in the more realistic model used here. This clearly indicates that NH_3 is not a suitable model for imidazole and explains easily the large barrier values proposed, even recently, in the literature.[28] Another factor that certainly concurs to make the barrier very small is the increase of hydrogen-bond strength in the transformation $m_1 \rightarrow ts_1$. This is observed for the interaction N_1–$H \cdots O_7$ ($H \cdots O_7$ varies from 3.693 to 2.993 Å) and the interaction O_1–$H \cdots O_3$, where $H \cdots O_3$ changes from 2.023 to 1.995 Å. The transition state ts_1 leads to a new intermediate m_2 (see Figure 4), where the O_1–$C(CO_2)$ bond is completed (1.421 Å). The newly formed bicarbonate fragment behaves here like a bidentate ligand that forms two simultaneous bonds (O_1–$Zn = 2.172$ Å and O_7–$Zn = 2.220$ Å) with the metal ion and actually makes m_2 a pentacoordinated

zinc complex. The deep water moves only slightly away from the position observed in m_1 and ts_1. However, this molecule now forms an additional hydrogen bond with the external bicarbonate oxygen O_6 ($O_6 \cdots H-O_2 = 2.141$ Å), which is simultaneously involved in an additional hydrogen interaction with the threonine N_1–H fragment ($O_6 \cdots H-N_1 = 1.967$ Å). Also, the geometry transformation leading to m_2 determines a strengthening of two already existing hydrogen bonds: that between the glutamate residue and the threonine OH group ($O_4 \cdots H-O_3$) and that involving this fragment and the bicarbonate OH fragment ($O_3 \cdots H-O_1$). This trend is evident from the values of the corresponding $O \cdots H$ distances, which vary from 1.762 and 2.023 Å in m_1 to 1.558 and 1.539 Å in m_2, respectively. The additional bonding interactions and the reinforcement of those already existing in m_1 are responsible for the strong stabilization that characterizes m_2, which is 33.5 kcal mol^{-1} lower than the asymptotic limit m_0.

B. Bicarbonate Rearrangement: Lipscomb and Lindskog Mechanisms. The internal proton shift in the bicarbonate fragment proceeds in two steps. The first step corresponds to a double proton transfer that involves the bicarbonate, the threonine residue, and the glutamate residue and requires the overcoming of a small barrier of 4.4 kcal mol^{-1} (transition state ts_2). In ts_2 (Figure 4), two protons are simultaneously migrating from the bicarbonate oxygen O_1 to the threonine oxygen O_3 and from this atom to the glutamate residue (oxygen O_4). The distances of the two protons from the two migrating terms are in the former case 1.315 and 1.144 Å ($H \cdots O_1$ and $H \cdots O_3$, respectively) and in the latter case 1.113 and 1.309 Å ($H \cdots O_3$ and $H \cdots O_4$, respectively). The rather low barrier can be partially explained by the presence of the water molecule that forms two hydrogen bonds with the two bicarbonate oxygen atoms O_1 and O_6. The strength of these bonds and thus their stabilizing effect clearly increases on passing from m_2 to ts_2 (the values of the $O_1 \cdots H$ and $O_6 \cdots H$ distances decrease in the same direction, i.e., from 2.543 and 2.141 Å to 2.470 and 2.002 Å, respectively). A further interaction that becomes more stabilizing on passing from m_2 to ts_2 is the hydrogen bond involving O_6 and the N_1–H group: the $H \cdots O_6$ distance is 1.967 Å in m_2 and 1.895 Å in ts_2. For the transformation $m_2 \rightarrow ts_2$, we have also evaluated the pure electrostatic effect of the Glu106 residue on the activation barrier. To compute this contribution we have simply considered the electrostatic interaction between the carbon and oxygen atoms of the Glu106 residue and the zinc and bicarbonate atoms (H, O_1, O_6, O_7, and C) in m_2 and ts_2. To this purpose we have used the net Mulliken atomic charges. This electrostatic potential becomes much more stabilizing on passing from m_2 (-0.7 kcal mol^{-1}) to ts_2 (-6.7 kcal mol^{-1}). Even if our approach only roughly estimates the electrostatic potential, these results suggest that this contribution is important in lowering the energy barrier. The double proton transfer leads to the intermediate m_3 (Figure 5), 2.8 kcal mol^{-1} higher than m_2, where the glutamate residue is protonated. The loss of a proton from the bicarbonate does not cause a considerable variation in the structure of the CO_3^{-2} ligand. m_3 can still be considered a pentacoordinated complex, the two Zn–O distances being 2.079 and 2.177 Å. The deep water maintains the two hydrogen bonds with the two atoms O_1 and O_6 ($H \cdots O_1 = 2.045$ Å and $H \cdots O_6 = 2.294$ Å), which are simultaneously involved in a network of hydrogen interactions with the O_3–H and N_1–H bonds. A second barrier
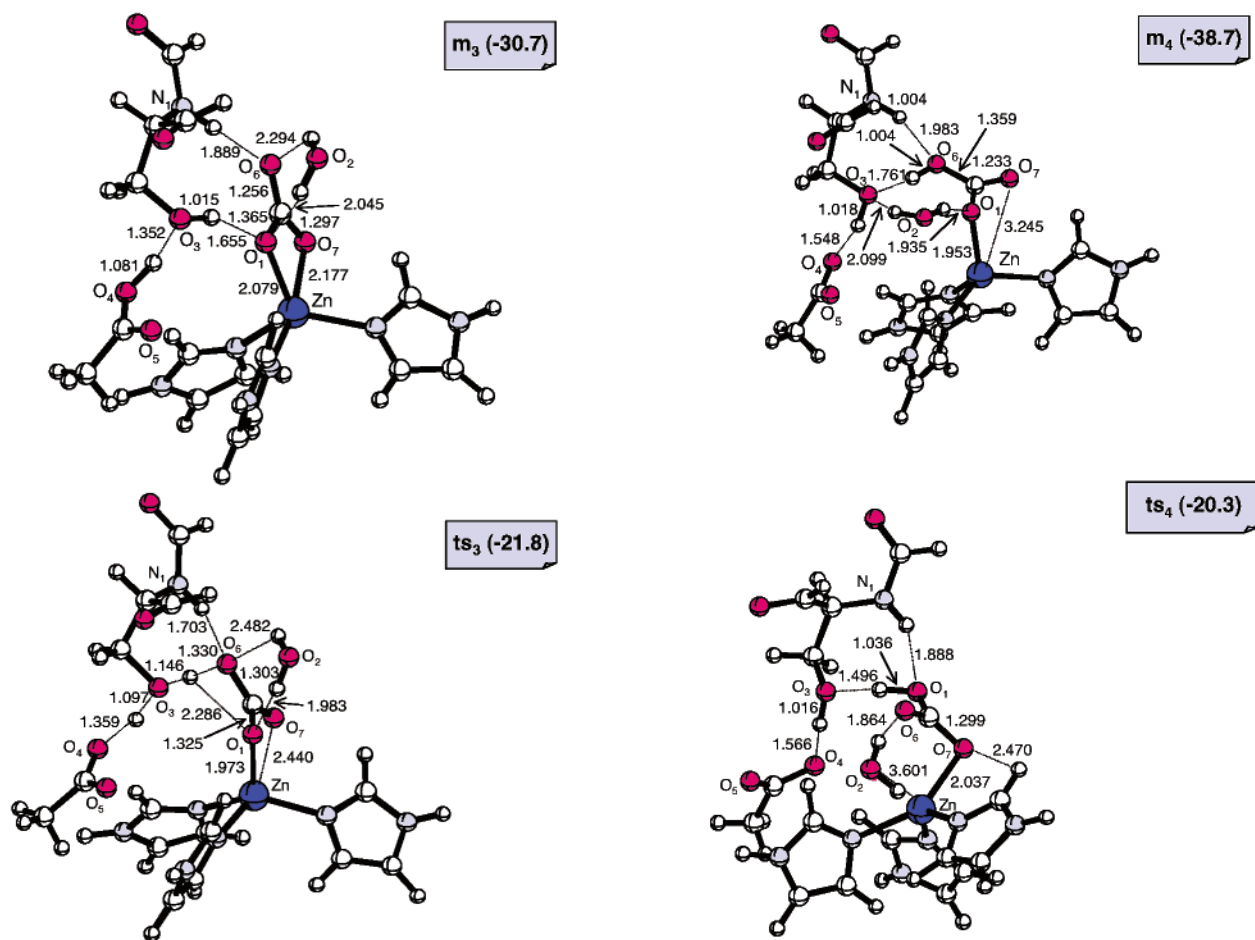
Figure 5. Schematic representation of the structures of the critical points m_3 and ts_3 (bond lengths in angstroms, angles in degrees). The energy values (kilocalories per mole) are relative to m_0.

Figure 6. Schematic representation of the structures of the critical points m_4 and ts_4 (bond lengths in angstroms, angles in degrees). The energy values (kilocalories per mole) are relative to m_0.

of 9.0 kcal mol^{-1} (transition state ts_3) must be overcome to transfer back one proton from O_4 to O_3 and the other from O_3 to O_6. In ts_3 (Figure 5) the $Zn-O_7$ bond is becoming longer (2.440 Å) and the CO_3 moiety is rotating around the $Zn-O_1$ bond to make easier the $O_3 \rightarrow O_6$ proton transfer. The final arrangement corresponds to the intermediate m_4 (Lipscomb intermediate, Figure 6), which is 5.2 kcal mol^{-1} lower in energy than m_2. m_4 is a four-coordinated complex where the $Zn-O_1$ bond is much shorter (1.953 Å) than in m_2 and the $Zn-O_7$ is now almost completely broken (3.245 Å). The deep water has moved from the position kept in m_2 and m_3 and is now bridging the two oxygen atoms O_1 and O_3 via two simultaneous hydrogen bonds (H···O_1 = 1.935 Å and H···O_3 = 2.099 Å). It is interesting to outline that this molecule now has a suitable orientation to attack the metal atom, which, after the trasfor-mation, has a vacant coordination site. The double-proton-transfer mechanism discussed here is in some ways similar to the proton shuttle mechanism, involving Thr199 and Glu106, suggested to explain the deprotonation of the zinc-bound water (see ref 16 and references therein).

An alternative reaction path directly leads from m_2 to m_4 through a rotation around the $C-O_7$ bond (Lindskog mecha-nism). In the corresponding transition state ts_4 (Figure 6), a complicated reorganization of the hydrogen-bond network and a motion of the water molecule from its position in m_2 to the final site determined in m_4 is evident. Since ts_4 has a barrier of

13.2 kcal mol^{-1}, the two reaction channels (i.e., the one-step $m_2 \rightarrow ts_4 \rightarrow m_4$ and the two-step $m_2 \rightarrow ts_2 \rightarrow m_3 \rightarrow ts_3 \rightarrow m_4$ channels) can effectively compete. These results are significantly different from the data obtained by other authors who found for the direct proton transfer a highly disfavored mechanism with a large barrier and indicated the internal rotation as the preferred mechanism.[28,29] These different conclusions are certainly due to the presence in our model system of the two residues Glu106 and Thr199 that we have demonstrated to be directly involved in the proton-transfer process.

C. Attack of the Water Molecule. We have also examined the attack of the water molecule on the bicarbonate−zinc complex m_4. We have already pointed out that the water oxygen lone pairs have here a suitable orientation to attack the metal. We have located a transition state (ts_5) where the newly formed O_2-Zn bond is 2.425 Å and the O_1-Zn bond becomes slightly longer (2.073 Å) than in m_4 (1.953 Å). It is interesting to note that ts_5 (see Figure 7) does not lead directly to the expulsion of the bicarbonate, as suggested elsewhere. In contrast, after overcoming a small barrier of 3.8 kcal mol^{-1}, we observe again the formation of a pentacoordinate zinc complex (m_5) where both the water and the bicarbonate are firmly bonded to the metal (the two O_2-Zn and O_1-Zn bonds are 2.213 and 2.225 Å, respectively). m_5 (represented in Figure 7) is slightly higher in energy (about 1.7 kcal mol^{-1}) than m_4. This destabilization is probably due to the loss of some stabilizing hydrogen bonds ($O_6-H\cdots O_3$ and $O_6\cdots H-N_1$) after the transformation $m_4 \rightarrow m_5$

Figure 7. Schematic representation of the structures of the critical points **ts₅** and **m₅** (bond lengths in angstroms, angles in degrees). The energy values (kilocalories per mole) are relative to **m₀**.
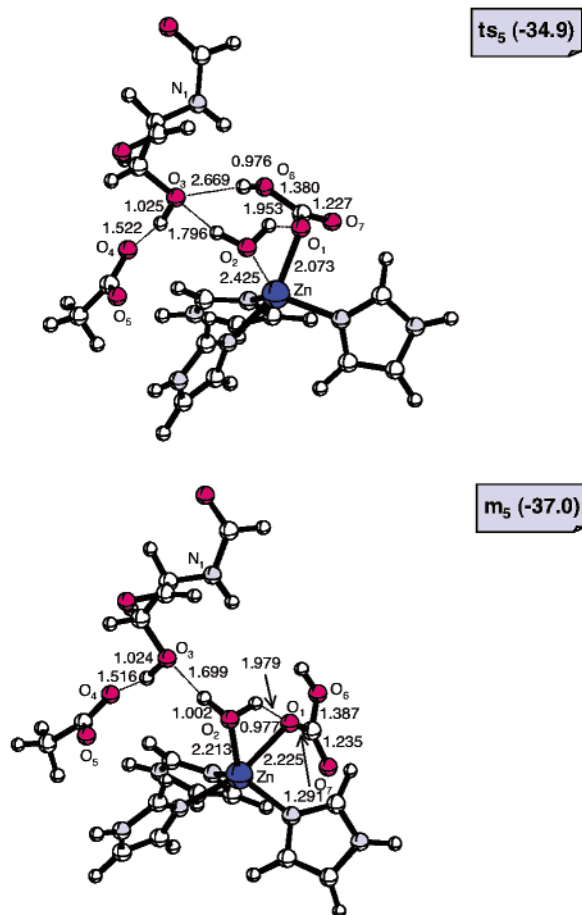

Figure 8. Schematic representation of the structures of the critical points **ts₆** and **m₆** (bond lengths in angstroms, angles in degrees). The energy values (kilocalories per mole) are relative to **m₀**.

that is only partially compensated by the new hydrogen bond between the water and the bicarbonate (O_2–H···O_1, where H···O_1 = 1.979 Å). A conformational rearrangement of **m₅** to an almost degenerate intermediate **m₆** (only 0.8 kcal mol⁻¹ lower in energy, Figure 8) is possible. This transformation corresponds to a rotation around the Zn–O_1 bond but requires the overcoming of a barrier of 8.6 kcal mol⁻¹. The structure of the intermediate **m₆**, even if degenerate to **m₅**, is of some interest. The polar tips of the bicarbonate moiety (O_7 and O_6–H) point now toward the two threonine residues Thr199 and Thr200. This structural arrangement should make easier the expulsion of the bicarbonate fragment (stabilization of the corresponding transition state) by interaction with the OH and NH groups of Thr199 and Thr200. Thr200 has not been considered in the present model yet, but its importance in the bicarbonate expulsion process is under investigation.

D. Effect of the Glutamate Residue. We discuss here the mechanism of the bicarbonate internal rearrangement in the absence of the Glu106 fragment (model II, **m₂*** → **m₄*** transformation). The two energy profiles obtained for the direct proton transfer and the alternative rotation mechanism are reported in the inset of Figure 2 (model II). The corresponding critical points are represented in Figures 9 and 10.

The starting intermediate **m₂*** (Figure 9) is similar to **m₂** found in model I. In **m₂*** the two zinc–oxygen bonds are 2.338 Å (Zn–O_1) and 2.097 Å (Zn–O_7): thus **m₂*** can be considered again a pentacoordinated zinc complex. The most relevant
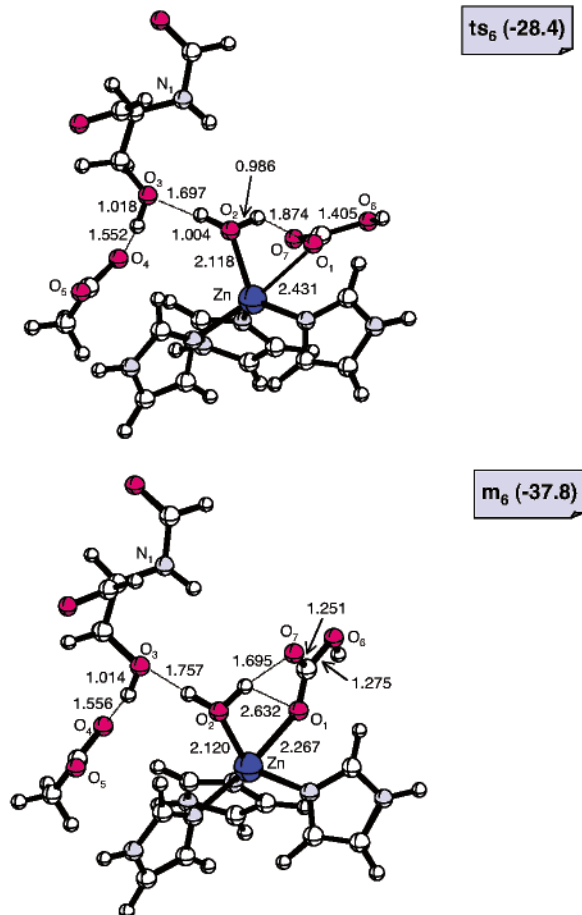
difference with respect to **m₂** is the position of the water molecule, which is now closer to the threonine residue. The deep water forms two hydrogen bonds with the N_1–H group: the O_2···H–N_1 interaction (H···O_2 = 2.422 Å) and the O_6···H–O_2 interaction (O_6···H = 2.715 Å). The proton transfer from O_1 to O_6 is now a one-step process (transition state **ts₂***) that requires the overcoming of a large activation barrier (about 32.3 kcal mol⁻¹), in agreement with previous computations reported in the literature.[28,29] The structural features of **ts₂*** can explain this large barrier. In the transition state, the migrating proton strongly interacts with the oxygen of the threonine OH group (O_3). Thus O_3 can be considered an oxygen atom with a formal positive charge, which certainly is a nonconvenient bonding situation. Furthermore, to undergo the proton transfer in one step, both the O_1 and O_6 oxygen atoms of the bicarbonate fragment must move toward the OH group, and this motion causes a significant weakening of the Zn–O_7 bond (it becomes 2.526 Å) and thus a destabilization of the complex. This structural deformation was not necessary in **ts₂** (model I), where only the oxygen O_1 was initially involved. However, it is interesting to point out that the second step of the proton transfer described in model I was characterized by a larger activation barrier (9.0 kcal mol⁻¹) than the first step. This is in agreement with a partial distortion of the bicarbonate and a consequent weakening of the Zn–O_7 bond (2.440 Å).

The alternative pathway (rotation) is characterized by the transition state **ts₄*** (Figure 10) and has an activation barrier of
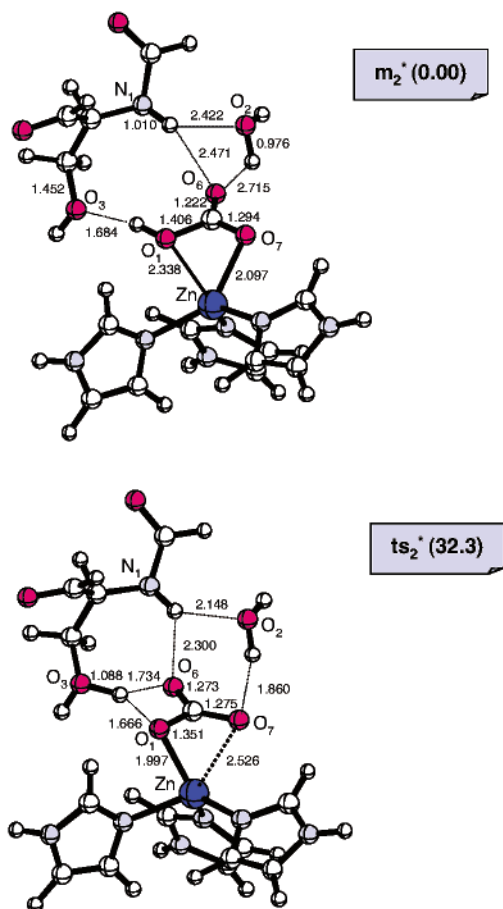
Figure 9. Schematic representation of the structures of the critical points m_2^* and ts_2^* (bond lengths in angstroms, angles in degrees). The energy values (kilocalories per mole) are relative to m_2^*.
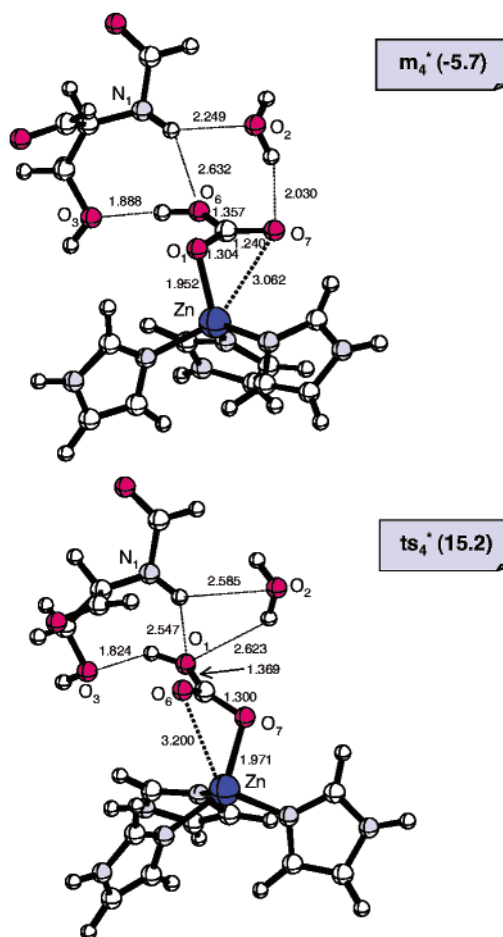

Figure 10. Schematic representation of the structures of the critical points m_4^* and ts_4^* (bond lengths in angstroms, angles in degrees). The energy values (kilocalories per mole) are relative to m_2^*.

15.2 kcal mol^{-1}. Thus, in model II, where the glutamate residue is missed, the rotation is strongly favored with respect to the direct proton transfer. The transition state ts_4^* differs from ts_4 for the position of the water molecule. This molecule approximately remains in the same place found in m_2^* but now has the two hydrogen atoms that point toward the N_1-H group and the O_1 atom and form two weak hydrogen bonds, i.e., $N_1-H\cdots O_2$ ($H\cdots O_2 = 2.585$ Å) and $O_1\cdots H-O_2$ ($O_1\cdots H = 2.623$ Å). A further difference with respect to ts_4 is found in the $O_3\cdots H-O_1$ hydrogen bond, which becomes significantly weaker in ts_4^*, the $O_3\cdots H$ distance being now 1.824 Å. This weakening can be responsible for the increase of the rotation barrier with respect to model I (13.2 kcal mol^{-1}).

E. Effect of the Protein Environment. The values of the activation energies obtained in the presence of solvent effects are reported in parentheses in Figure 2. The barrier for the nucleophilic attack ($m_1 \rightarrow ts_1$) remains very small, being now 1.4 kcal mol^{-1}. This enforces the hypothesis that this attack cannot be the rate-determining step of the catalysis. More interestingly, the relative importance of the two mechanisms for the bicarbonate rearrangement is not affected by the solvent effect. The two barriers for the proton transfer ($m_2 \rightarrow ts_2$ and $m_3 \rightarrow ts_3$) change only slightly (from 4.4 and 9.0 kcal mol^{-1} to 3.9 and 10.6 kcal mol^{-1}, respectively), and the barrier for the rotation varies from 13.2 to 14.4 kcal mol^{-1}. It is important to point out that the Lipscomb intermediate (m_4) remains significantly more stable than the Lindskog intermediate (m_2), the

energy lowering caused by the structural rearrangement being now 4.9 kcal mol^{-1}. The activation energy for the formation of the pentacoordinated complex due to the water attack is now 5.5 kcal mol^{-1}, a value that does not differ too much from that previously determined of 3.8 kcal mol^{-1}. A more significant difference is found in the final conformational rearrangement of the pentacoordinated complex, which becomes now much easier since it requires an activation of only 2.7 kcal mol^{-1}.

The results obtained for model II are not affected by the inclusion of the protein environment effects. Again, in the absence of Glu106, the Lindskog mechanism (rotation) becomes much easier than the Lipscomb mechanism (proton transfer), with the two corresponding activation barriers being 14.9 and 28.1 kcal mol^{-1}, respectively.

F. Effect of Basis Set Accuracy. The energy values, relative to reactants, obtained with the DZVP basis on the whole system are collected in Table 1. For the sake of comparison we have also reported the values obtained with the LDBS approach. The most evident effect of the larger basis is a shift of the entire energy profile to higher energy values. Accordingly, the energy lowering associated with the formation of the encounter complex m_1 is now only 6.0 kcal mol^{-1} and the two final complexes m_5 and m_6 are respectively 19.3 and 25.7 kcal mol^{-1} lower than the asymptotic limit. However, these changes do not affect significantly the conclusions reached in the previous sections. The barrier for the initial nucleophilic attack is negligible, i.e.,

Table 1. Relative Energy Values[a] of the Critical Points Obtained for Models I and II by the LDBS Approach and the DZVP Basis on the Whole System

	LDBS	DZVP		LDBS	DZVP
		Model I[b]			
m_0	0.0	0.0	m_4	−38.72	−21.89
m_1	−17.53	−6.03	ts_4	−20.25	3.20
ts_1	−16.91	−5.99	ts_5	−24.88	−17.44
m_2	−33.50	−18.19	m_5	−36.97	−19.30
ts_2	−29.11	−15.81	ts_6	−28.41	−10.04
m_3	−30.73	−18.41	m_6	−37.84	−25.70
ts_3	−21.76	−6.20			
		Model II[c]			
m_2*	0.00	0.00	ts_4*	15.25	17.51
ts_2*	32.34	28.88	m_4*	−5.71	−2.77

[a] Energies are given in kilocalories per mole. LDBS, locally dense basis sets; DZVP, local spin density-optimized basis set of double-ζ quality that includes polarization functions. [b] The absolute energies of **m_0** are −3451.749 50 au (LDBS) and −3464.395 35 au (DZVP). [c] The absolute energies of **m_2*** are −3223.595 33 au (LDBS) and −3235.706 96 au (DZVP).

only 1.2 kcal mol^{-1}. The two barriers for the proton transfer are 2.4 and 12.3 kcal mol^{-1}, while that required by the rotation significantly increases and becomes 21.6 kcal mol^{-1} (13.2 kcal mol^{-1} with the LDBS approach). Thus, the larger basis set definitely points to the Lipscomb mechanism as the preferred pathway to afford the bicarbonate rearrangement. To estimate the effect of the geometry optimization on this barrier, we have reoptimized the Zn−N bond lengths at the DZVP level for both the **m_2** and **ts_4** critical points. We have found that these bonds do not vary dramatically. They become longer by 0.05 and 0.07 Å in **m_2** and **ts_4**, respectively, and the corresponding barrier changes only slightly, becoming 20.9 kcal mol^{-1}. This suggests that single-point DZVP computations on the LDBS structures can provide a reliable estimate of the various activation energies. The significant variation of the **m_2** − **ts_4** energy difference on passing from the LDBS to the DZVP level (not observed for the other energy barriers) could be due to the hydrogen bond involving O_7 and one imidazole hydrogen (see Figures 4 and 6). This bond becomes longer and thus less stabilizing in the transition state (the O_7···H distance varies from 2.406 to 2.470 Å), and its effect is probably better evaluated with the DZVP basis that includes polarization functions on the hydrogen atoms. The transformation **m_2** → **ts_4** leads again to a more stable intermediate: **m_4** is now 3.7 kcal mol^{-1} lower in energy than **m_2**. Similar results to those previously discussed are obtained for the two final steps along the energy profile (**m_4** → **ts_5** and **m_5** → **ts_6**), the corresponding barriers being 4.4 and 9.3 kcal mol^{-1}, respectively.

The barriers for the Lindskog and Lipscomb mechanisms are not seriously affected by the basis set accuracy when we consider model II. In the former case (rotation) we have found a value of 17.5 kcal mol^{-1}, and in the latter (proton transfer) the barrier becomes 28.9 kcal mol^{-1}. Thus, once again, the computational results emphasize the key role played by the glutamate residue in determining the preferred mechanism.

4. Conclusions

In this paper a DFT study has been carried out on some important aspects of the catalytic cycle of the carbonic anydrases. In particular, the mechanism of the nucleophilic attack of zinc-bound OH on the CO_2 molecule and the internal

rearrangement of the resulting bicarbonate fragment bonded to the metal have been carefully examined. The most significant results can be summarized as follows:

(i) A stable encounter complex between CO_2 and the zinc-bound hydroxide forms without any barrier in the first step of the process. The formation of this complex has the effect of desolvating the Thr199 residue (the deep water is pushed away) and leads to a rough orientation of the substrate for the subsequent nucleophilic attack. These results are similar to those discussed in refs 28 and 29, even if the orientation of CO_2 is determined in our cases by the presence of the deep water molecule.

(ii) The barrier required by the nucleophilic attack is very low in all cases (only 0.6 or 1.2 kcal mol^{-1}). This is somewhat different from the results obtained by other authors, who found larger values.[28,29] The small barrier found here is mainly determined by the high nucleophilic character of the zinc-bound hydroxide, which in turn depends on the metal imidazole ligands. Thus, the nucleophilic attack cannot correspond to the rate-determining step of the catalytic cycle.

(iii) In the presence of the two Glu106 and Thr199 residues the direct proton transfer (Lipscomb mechanism) becomes a two-step process, which proceeds via a proton relay network (4.4 and 9.0 kcal mol^{-1} are the corresponding activation barriers). This pathway can effectively compete with the rotation (Lindskog mechanism), which has a barrier of 13.2 kcal mol^{-1}. This competition becomes more evident when we consider the results obtained with a larger base. In this case the two-step proton transfer is decidedly favored. These evidences are somewhat similar to the conclusions reached by Bertran and co-workers.[21] They suggested that both mechanisms can be present and are acceptable to explain the experimental data. The fast proton transfer found here is basically due to the effect of the residue Glu106, which stabilizes an intermediate situation where the glutamate fragment is protonated (**m_3**). The computational evidence obtained in model II, where this residue is absent, stresses the key mechanistic role played by Glu106. In that case the proton-transfer barrier becomes much larger (32.3 kcal mol^{-1}) and the Lindskog mechanism becomes highly favored.

(iv) The attack of the water molecule and the expulsion of the bicarbonate fragment do no occur simultaneously. Two five-coordinated zinc complexes, involving both H_2O and HCO_3^- as ligands, have been located. Other five-coordinated zinc complexes, such as **m_2** (Lindskog intermediate) and **m_3**, are involved in the catalysis.

(v) The computations carried out with the inclusion of solvent effects, which emulate the protein environment, provide the same mechanistic scenario obtained with the gas-phase model.

Supporting Information Available: Tables S1 (model I) and S2 (model II), listing geometrical parameters and total energy values for the various critical points (print). This information is available free of charge via the Internet at http://pubs.acs.org.

JA030336J